Journal of Environmental Chemical Engineering 9 (2021) 106624

Contents lists available at ScienceDirect

Journal of Environmental Chemical Engineering

journal homepage: www.elsevier.com/locate/jece

Screening the growth inhibition mechanism of sulfate reducing bacteria by chitosan/lignosulfonate nanocomposite (CS@LS) in seawater media

Kashif Rasool [a], Ravi P. Pandey [a], P. Abdul Rasheed [a], Tricia Gomez [a], Enas S. Al-Absi [b,c], Gheyath K. Nasrallah [b,c], Khaled A. Mahmoud [a,*]

[a] Qatar Environment and Energy Research Institute (QEERI), Hamad Bin Khalifa University, Qatar Foundation, P.O. Box 34110, Doha, Qatar
[b] Biomedical Research Center, Qatar University, Doha 2713, Qatar
[c] Department of Biomedical Science, College of Health Sciences, Member of QU Health, Qatar University, Doha 2713, Qatar

ARTICLE INFO

Editor: Yang Liu

Keywords:
Green biocides
Chitosan/Lignosulfonate nanocomposite
SRBs biofilm
Toxicity

ABSTRACT

Sulfate-reducing bacteria (SRBs) induced biofilm formation is a global industrial concern due to its role in the development of microbial-induced corrosion (MIC). Herein, we have developed a biodegradable chitosan/lignosulfonate nanocomposite (CS@LS) as an efficient green biocide for the inhibition of SRBs biofilms. We investigated in detail the inhibition mechanism of SRBs by CS@LS in seawater media. Stable CS@LS-1:1 with 150–200 nm average size, and zeta potential of + 34.25 mV was synthesized. The biocidal performance of CS@LS was evaluated by sulfate reduction profiles coupled with analysis of extracted extracellular polymeric substances (EPS) and lactate dehydrogenase (LDH) release assays. As the nanocomposite concentration was increased from 50 to 500 μg/mL, the specific sulfate reduction rate (SSRR) decreased from 0.278 to 0.036 g-sulfate/g-VSS*day showing a relative sulfate reduction inhibition of 86.64% as compared to that of control. Similarly, the specific organic uptake rate (SOUR) decreased from 0.082 to 0.039 0.036 g-TOC/g-VSS*day giving a relative co-substrate oxidation inhibition of 52.19% as compared to that of control. The SRBs spiked with 500 μg/mL CS@LS showed a reduction in cell viability to 1.5×10^6 MPN/mL. To assess the biosafety of the nanocomposite on the marine biota, the 72-hours acute toxicity assays using zebrafish embryo model revealed that the LC_{50} for the CS@LS was 103.3 μg/mL. Thus, CS@LS can be classified as environment friendly. The nanocomposite showed long-term stability and excellent antibacterial properties against SRBs growth and is thus potentially useful for combating the problems of biofilm growth in harsh marine and aquatic environments.

1. Introduction

Biofilm causing microbiologically influenced corrosion (MIC) is a major problem in many industries including oil and gas. Corrosive biofilms which consist of microbial constituents embedded in a highly hydrated, extracellular polymeric matrix on metal surfaces are formed by different anaerobic microorganisms [1]. Apart from abiotic corrosion, biocorrosion which is estimated at ~20% of total global corrosion affects the lifetime of various industrial materials and equipment [2]. Among the anaerobic microorganisms, sulfate-reducing bacteria (SRBs) are the most abundant bacteria commonly associated with microbial corrosion on metal surfaces [3]. The presence of SRBs in the anaerobic marine environment can significantly accelerate the biocorrosion of metal and its alloys including copper, carbon steel, and stainless steel [4]. The formation of SRBs biofilm can deteriorate metal surfaces, which stimulate metal sulfide precipitation and result in intergranular corrosion. Seawater, commonly used to enhance the oil recovery as injecting water, has high sulfate concentrations where anaerobic conditions will eventually prevail and SRBs can metabolize hydrocarbons and thereby intensify the biocorrosion of metal structures under anaerobic conditions [5–7]. A traditional strategy to control MIC is the application of biocides to inhibit the microorganisms in the aqueous environment. However, majority of these traditional biocides are not environmentally friendly and sometimes less effective when microorganisms are imbedded into biofilm matrix, preventing biocides from penetrating into the biofilm [8–10]. A lot of effort has been made toward the sustainable production of alternative sustainable, environment friendly bactericidal agents to address concerns over conventional biocides.

Several nanomaterials (NMs) composed of metal, metal oxides (e.g. Ag, Cu, ZnO, Ti, Ni), natural polymers, and carbon-based materials have

* Corresponding author.
E-mail address: kmahmoud@hbku.edu.qa (K.A. Mahmoud).

https://doi.org/10.1016/j.jece.2021.106624
Received 24 June 2021; Received in revised form 27 September 2021; Accepted 17 October 2021
Available online 21 October 2021

been recognized as effective biocide against a variety of microorganisms [3,11–16]. However, there is a concern that after releasing into the environment, these NMs can cause toxicity to living systems [17]. So, there is a need to develop NMs which are stable, have excellent antibacterial activity, and are sustainable and environmentally benign. Much work in today's studies of engineered nanoparticles is focused on green NMs derived from natural biopolymers.

Biopolymers are attractive candidates to create high-performance and environmentally friendly functional reactive compounds. Chitosan (CS) is inexpensive, non-toxic, biocompatible, and biodegradable natural polymer obtained from biomass and possesses antibacterial properties and hydrophilic nature [18,19]. CS contains free amino groups, which impart a net positive charge favoring ionic interaction with many negatively charged surfaces, or polymers, which have made it of great interest for applications as antibacterial agents [20,21]. Lignosulfonic acid (LS) is one of the lignin derivatives, which is produced in large quantities as waste from paper pulping industry. It has several industrial applications including good antibacterial activity [22].

In our recent work, we reported an innovative one-step process for the synthesis of chitosan/lignosulfonate nanocomposite (CS@LS), as a "green" biocide, under solvent-free conditions [23]. We have employed a versatile method to form the stable cross-linked chitosan-lignosulfonate (CS/LS) nanospheres. The optimum composite structure of CS@LS-1:1 form 150–200 nm nanospheres with high mechanical, thermal, and bactericidal properties against aerobic and anaerobic bacteria. Particularly, a 100 mg/L CS@LS-1:1 was able to inhibit SRBs growth, as demonstrated by 48.8% lower sulfate reduction.[23] Moreover, a 500 $\mu g \cdot mL^{-1}$ of the CS@LS nanospheres were highly effective for the inhibition of mixed sulfate-reducing bacteria (SRBs) culture, thereby controlling the microbiologically influenced corrosion (MIC) on carbon steel up to a maximum of 85% indicated by a two-fold increase of charge transfer resistance (R_{ct}) on the carbon steel coupons.[24] However, the antibacterial mode of action of CS nanocomposites against complex bacterial consortia has not been fully investigated or understood. It is expected that CS-based organic biocides could efficiently inhibit biofilm growth as they would adsorb onto metal surfaces through heterocyclic elements (such as nitrogen, oxygen, sulfur, and phosphorus), multiple bonds, or aromatic rings and block the active sites, thus working as an inhibitor for the biofilm growth [25,26].

In the present work, we evaluate in more detail the biological activity of CS@LS at different stoichiometric ratios against SRBs biofilm in seawater media. The antibacterial effect of CS@LS on the sulfate reduction process of anaerobic SRBs biofilm were investigated at various concentrations and compared to that of CS and LS by the analysis of extracellular polymeric substances (EPS) of biofilms coupled with lactate dehydrogenase (LDH) release assay and scanning electron microscopy (SEM). The safe use of these nanoparticles in the aquatic environment was tested using the zebrafish acute toxicity assays, a cheap and reliable aquatic model that is increasingly used for drug and nanoparticle toxicity testing [27].

2. Materials and methods

2.1. Materials

CS (low molecular weight, deacetylation degree of 85%), sodium lignosulfonate (LS), diethylamino benzaldehyde (DEAB), N-Phenylthiourea (PTU), CH_2O, and E3 media ingredient including KCl, NaCl, $CaCl_2 \cdot 2H_2O$, and $MgSO_4 \cdot 7H_2O$ were obtained from Sigma Aldrich. SRBs culture was enriched from biofilm sludge obtained from local industry in Qatar. All the other chemicals and reagents were of analytical grade and used without additional treatment.

2.2. Preparation and characterization of CS@LS nanocomposite

The procedure for the preparation of CS@LS nanocomposite (NC) was reported earlier [23,24]. Briefly, CS (10 mg/mL) was dissolved in DI water (1% w/w) with acetic acid and overnight stirring at 25 °C using a magnetic stirrer. The resulting solution was filtered using a 0.45 μm filter (Millipore, USA) to remove any residues followed by adjustment of the pH to 5.0 using 10 N NaOH. An aqueous solution of LS (10 mg/mL) was made by dissolving LS in DI water. A cross-linking agent was prepared by adding 0.54 g, 1.5 g, and 1.25 mL of formaldehyde, Na_2SO_4, and H_2SO_4, respectively, in 4.7 mL of DI water. CS@LS nanospheres were synthesized by adding the above prepared CS and LS solution at different stoichiometric ratios of 1:1, 1:2, and 2:1, respectively, at room temperature (25 °C) under magnetic stirring. Cross-linking agent (450 μL) was added proportionally using a syringe and continued to stir for another 30 min. Finally, the resulting solution was centrifuged at 10, 000 rpm and resuspended in DI water. The centrifugation process was repeated five times to remove any unused cross-linker to get the CS@LS hybrid. The obtained CS@LS hybrids are named as CS@LS-1:1, CS@LS-1:2, and CS@LS-2:1. Synthesized NC was characterized using wide-angle XRD (Bruker AXS, Germany) FT-IR spectrum (Nicolet™ iS50 FTIR Spectrometer), scanning electron microscopy (FEI Quanta 650 FEG SEM), and transmission electronic microscopy FEI Talos F200X TEM microscope as discussed earlier [28].

2.3. Aggregation and stability studies of CS@LS nanospheres

The stability of CS@LS was evaluated using LUMiCheck®Germany which works on the back-scattering principle. The CS@LS NC suspensions were prepared by adding CS@LS-2:1, CS@LS-1:1, and CS@LS-1:2 in simulated Postgate media to reach 100 μg/mL mass concentrations of the hybrid composites. One mL of suspension was transferred to quartz colorimetric cuvette and the sedimentation behavior was followed for 24 hrs. In a second assay, the effect of NC concentration on the aggregation and settlement of NC was evaluated by adding 20, 50, 100, 300, and 500 μg/mL of optimized CS@LS. Over time, the change in backscattering signal was used to indirectly characterize the aggregation of CS@LS. The backscattering (B) was determined after different time intervals and the aggregation of NC was calculated using Eq. (1).

$$\%\,\text{Aggregation}(A_t) = \frac{B_0 - B_t}{B_0} \times 100 \quad (1)$$

Where B_0 and B_t are the backscattering at an initial time and at any time interval t, respectively.

2.4. Enrichment of sulfate-reducing bacteria (SRBs) biofilm and biofilm inhibition studies

The SRBs sludge culture used in this study was developed from biofilm samples collected from the local industry as described earlier [29]. Antibacterial activity of synthesized NC against SRBs culture was investigated in batch assays. The glass bioreactors containing 150 mL of simulated inject water and SRBs biofilm (200 mg.VSS/L) were exposed with 100 μg/mL of LS, CS, CS@LS-1:1, CS@LS-2:1, and CS@LS-1:2 each and incubated at 35 °C and 150 rpm shaking speed in an anaerobic environment. A batch reactor without any (NMs) was used as a control. An aliquot was taken at specific time intervals and was centrifuged at 10, 000 rpm for 10 min. The supernatant obtained was used to determine co-substrate oxidation and sulfate reduction. The material which showed the highest inhibition of SRBs activity was considered as the optimal one for further studies. Effect of concentrations of NC on SRBs biofilm activity was investigated by adding 10, 20, 50, 100, and 250 μg/mL of CS@LS while keeping sulfate and total organic carbon (TOC) concentrations constant at 1000 and 650 mg/L, respectively, for each assay. All assays were conducted in triplicate and average values were reported.

2.5. Cell staining and flow cytometer analysis

Cell suspensions after reaction were collected and stained with SYTO 9 and propidium iodide (PI) simultaneously using LIVE/DEAD ® BacLight™ Kit. 1 mL of SRBs biomass after reaction with NC was centrifuged at 10,000*g* for 3 min. The supernatant obtained was discarded and pellet was collected and resuspended in PBS buffer and washed thrice using the same protocol. A staining mixture was obtained by adding PBS buffer (987 μL), SYTO 9 (1.5 μL of 3.34 mM) and propidium iodide (1.5 μL of 30 mM) in a flow cytometry tube. SRBs biomass was stained by adding10 μL of washed suspension into the staining solution, mixed and incubated in the dark at 25 °C for 20 min. Analysis of stained cells was performed using a flow cytometer (BD Accuri™ C6 BD Biosciences, CA).

2.6. SEM imaging, LDH release assay, and biofilm analysis

The effect of CS@LS on SRBs biomass structure was investigated by SEM analysis using the method as discussed earlier [30]. Briefly, sludge samples were fixed with 2% glutaraldehyde solution for 2 h followed by dehydration with a series of ethanol concentrations. Finally, samples were washed with water and stored under dry nitrogen before analysis. The samples were gold sputter coated and analyses were carried out with FEI Quanta 650 FEG (Hillsboro, OR, USA) SEM. The cell membrane integrity of SRBs biofilm exposed to CS@LS in the seawater was investigated using LDH release assay. Standard procedure was carried out as per the manufacturer's guidelines using 1 mL of SRBs biomass suspension treated with 250 μg/mL of CS@LS. The constituents of EPS were studied before and after the exposure to CS@LS NC. SRBs biomass suspension was collected from all the batch assays and EPS was extracted as discussed in our earlier study [31]. Extracted EPS samples were stored at −20 °C until further characterization was performed. Concentrations of important constituents of the biofilm EPS were evaluated as described earlier [31].

The performance of the NC for SRBs growth inhibition was monitored by studying TOC, volatile suspended solids (VSS), sulfide, sulfate, and sulfite. The aqueous suspension (2 mL) was collected at different time intervals and centrifuged at 10,000 rpm for 15 min. The supernatant was collected and used for further measurements. TOC was measured by a TOC analyzer (Shimadzu). Sulfate and sulfite were analyzed by ion chromatography (DX ICS-5000 Dionex, USA). VSS was measured following the standard methods (APHA, 1998). Dissolved sulfide was analyzed immediately after sample collection by titrimetric method (APHA, 1998).

2.7. Zebrafish culture and acute toxicity assay

10X stock solutions of PBS, Egg water, PTU, and methylene blue were prepared as described earlier [29,32]. To avoid the aggregation and to reach the maximum dispersion, a stock solution 1.0 g/L for the CS@LS or CS, LS were prepared by adding 0.01 of each compound to 10 mL 1X PTU-E3 media and probe sonicated for 5 min for 2 cycles. The stock solutions were then more diluted to 25, 50, 100, 150, 200, 250 μg/mL at the time of the study. Wild-type zebrafish embryos (AB strain) were used in this study. Detailed information about our zebrafish aquatic system (Aquaneering, USA), the original source of the zebrafish, zebrafish culture, mating protocol, and animal protocol guidelines, can be obtained elsewhere [29,32–35].

For the acute toxicity assay, at 24-hours post-fertilization (hpf), embryos were dechorionated as described in [34]. Briefly, E3 media were removed and 0.5 mg/mL of pronase enzyme (Sigma, Germany) in 10 mL PTU-E3 media was added and incubated for 10 min at 28 °C until the chorion becomes soft. Then, embryos were washed 2–3 times with PTU-E3 medium until the embryos were released and free from the chorion. The healthy dechorionated embryos were selected for the acute nanoparticle exposure experiment. Embryos were placed in 12-multiwell plate, each well contains 3 mL of fresh PTU-E3 media containing (i) six different concentrations of CS@LS (25, 50, 100, 150, 200, and 250 μg/mL) (ii) positive control (PC) DEAB (0.1, 10, 100 μM), and (iii) PTU-E3 media alone as a negative control (NC), and incubated for additional 48 (until embryos reached 72-hpf). The mortality rate and teratogenicity (morphological deformities) were observed and recorded at 2-time point intervals (48 and 72-hpf) using a standard stereo microscope (Zeiss, Germany). The teratogenic effects of CS@LS were determined based on the normal embryo morphology of the negative control, and abnormal morphology defects in body size, heart and yolk edema, scoliosis, pigmentation, and movement problem of the positive control. Teratogenicity was scored at 72-hpf by calculating the number of dead and deformed embryos over the total number of normal embryos used in each concentration (50 embryos). The embryos were scored as dead if they showed coagulation of unfertilized eggs, no somite formation, lack of detachment of tail-bud from the yolk sac, and no heartbeat [34]. The median lethal dose (LC_{50}) was calculated using the Graph Pad Prism software as detailed in the earlier study [32]. Furthermore, the no observed effect concentration (NOEC) value was designated as the highest tested concentration with no statistically significant teratogenic score (<20% deformity and mortality), within the exposure period (24–72 hpf, total 48 h) when compared with the negative control.

3. Results and discussions

3.1. Preparation and characterization of CS@LS nanocomposites

The CS@LS NC were prepared by one-step synthesis of chemically cross-linked CS and LS according to our earlier reported method [23,24]. Fig. 1 depicts the SEM images of the synthesized CS@LS NC at different stoichiometric ratios. The CS@LS-2:1 and CS@LS-1:2 showed aggregated irregular-shaped nanoparticles, whereas, CS@LS-1:1 showed a very uniform spherical shape with an average diameter in the range of 150–200 nm (Fig. 1(A-C)). TEM images of CS@LS hybrids showed consistent results with SEM and confirmed the spherical morphology (Fig. 1(D-F)). Based, on our experimental results reported earlier, CS@LS-1:1 with ratio 1:1 (CS:LS) has been considered as the optimum ratio for preparing the NC [23] therefore it was selected as a model for further analysis. Fig. 1 (G) describes the XRD patterns of CS, LS, and CS@LS-1:1. It was observed that the XRD pattern of CS consisted of two major peaks at ca. ~10.0° and ~20.0°, which are typical fingerprints of crystal CS [28,29]. LS has a broad (002) graphite-peak centered near 2θ ~ 22° [30]. The CS@LS-1:1 NC showed a broad peak at 22.7°, which may be due to the formation of a new binary framework that could disrupt the original structure of both CS and LS [23,36]. In the composite, the peak at 10.0° disappeared, while the peak intensity at around 20.0° decreased indicated a more amorphous phase of the composite. The FTIR spectra of CS, LS, and CS@LS-1:1 are given in Fig. 1 (H). The characteristic absorption bands at 1654, 1381, and 1069 cm^{-1} are assigned to the C═O stretching (amide I), CH_3 symmetrical deformation, and the C-O stretching vibrations (C-O-C) of CS, respectively [37]. The FTIR spectrum of LS shows characteristics absorption bands at 1609, 1209, and 1044 cm^{-1} corresponding to the C═C stretch of phenyl, C-O stretch of –OCH_3, and S═O stretch of –SO_3Na, respectively [38]. The FT-ATR spectrum of CS@LS-1:1 showed an absorption band at ~1158 (sym. SO_2 stretch), and at ~1634 (-NH_2 bending vibration) and confirmed the presence of sulphonic acid groups and amine groups. The cross-linked structure of the CS@LS-1:1 composite was also confirmed by diether (–C–O–C–) absorption band at 1031 cm^{-1} [39]. Furthermore, a strong absorption band at ~1101 cm^{-1} attributed to the C-O stretch of CS and –OCH_3 groups.

Nanoparticle stability plays an important role in their bactericidal properties [40]. During the application of nanoparticles in aqueous suspensions, maintaining their colloidal stability is an important factor to avoid aggregation, as the formation of bigger aggregates results in loss of their bactericidal properties [41,42]. Nanoparticles can transform due

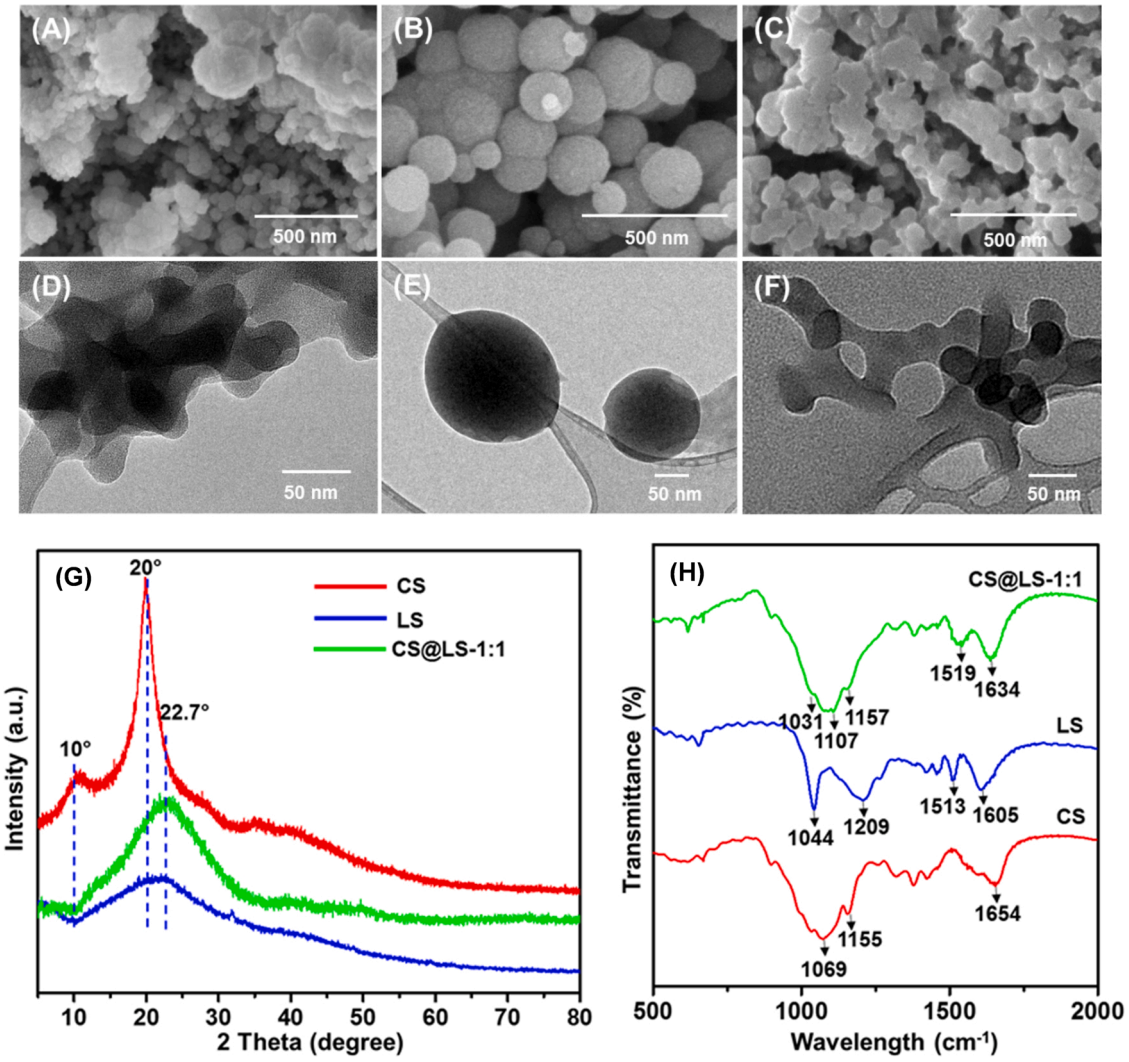

Fig. 1. SEM images (A) CS@LS-2:1 (B) CS@LS-1:1 and (C) CS@LS-1:2; TEM images (D)CS@LS-2:1 (E) CS@LS-1:1 and (F) CS@LS-1:2; (G) XRD pattern of CS, LS, and CS@LS-1:1 composite; and (H) FTIR spectra of CS, LS, and CS@LS-1:1 composite.

to several factors, such as aggregation, redox, surface moieties, and culture media reactions. These active changes sequentially affect the transport, and bactericidal characteristics of nanoparticles. So, it is critical to comprehend and characterize the stability of NC in the relevant reaction media. The trends of CS@LS aggregation were investigated in seawater matrix at different initial CS@LS stoichiometric ratios. The data showed that the rate of sedimentation was related to the ratio of CS and LS, which is shown by the relatively stable suspension of CS@LS-1:1 in growth media as compared to that of CS@LS-1:2 and CS@LS-2:1 NC (Fig. 2 (A). These results are in line with the SEM analysis

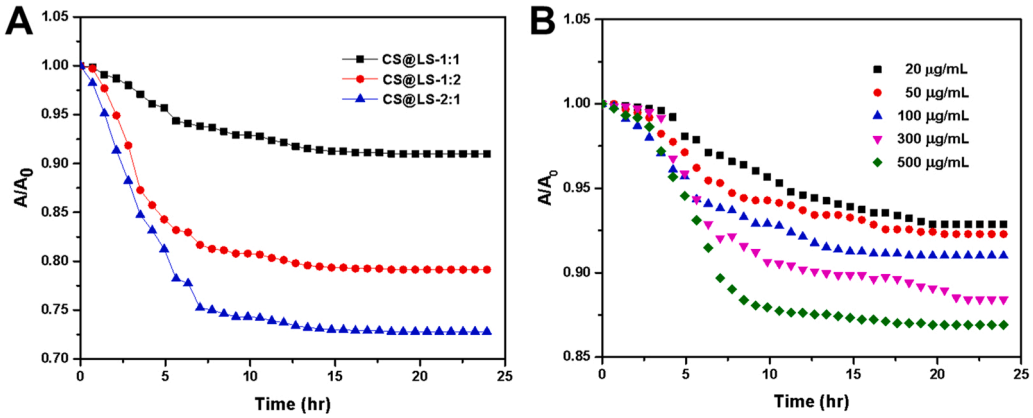

Fig. 2. Sedimentation plots for CS@LS over the time plotted at (A) CS@LS different ratios at a constant concentration of 100 µg/mL and (B) different initial concentrations of CS@LS-1:1 nanocomposite suspensions.

which shows that CS@LS-1:1 are well dispersed and uniform spheres whereas CS@LS-2:1 and CS@LS-1:2 showed aggregated irregular shaped nanoparticles. Fig. 2 (B) shows the sedimentation rates for the suspensions at different CS@LS-1:1concentrations. The B/B_0 ratio (where B_0 and B show the initial and at any time t backscattering, respectively) showed that the suspensions with lower concentrations of CS@LS were relatively more stable because the faster B/B_0changes, the less stable will be the suspension. The precipitation rate gradually increased with the time for initial 5 h with increasing CS@LS concentration to 500 μg/mL. After 5 hr of interaction time, there was no further sedimentation and the suspensions became stable.

3.2. Influence of synthesized nanocomposites on SRBs activity

The SRBs inhibitory activity in the anaerobic aqueous media was initially studied by exposing the bacteria to LS, CS, CS@LS-1:1, CS@LS-2:1, and CS@LS-1:2. To investigate the impact of different compositions and concentrations on the activity of SRBs consortia, sulfate reduction and organics oxidation were studied by residual sulfate and TOC analysis as shown in Fig. 3. In a control assay, the sulfate concentration was reduced from the initial 1000 mg/L to 35 mg/L after 85 h reaction time with more than 96% of sulfate reduction efficiency. The concentration of TOC decreased from 700.0 mg/L to 180.5 mg/L with an organic oxidation efficiency of 73.6%. The sulfate reduction efficiency was 82.0%, 88.78%, 53.8%, 65.26% and 76.81% in presence of 100 μg/mL of CS, LS, CS@LS-1:1, CS@LS-1:2 and CS@LS-2:1, respectively. It was observed that CS@LS-1:1 showed the highest decrease in sulfate utilization among all other composites (Figure3). Similarly, TOC removal efficiency profiles also showed similar trends and CS@LS-1:1 demonstrated the highest residual organics concentration with a co-substrate utilization efficiency of 54.26%. The biological sulfate reduction requires eight reducing equivalents, i.e., a minimum COD/sulfate ratio of 0.67 is needed theoretically for achieving a possible removal of sulfate [43]. That means, for each 0.96 g of sulfate present in bioreactor, 0.64 g of COD are consumed. However, the dominating microbial group in sulfidogenic environment is the fermentative acidogenic bacteria (FAB), during the acidogenic phase of metabolism. The FAB play a key role in degrading substrate to smaller organic compounds like ethanol, hydrogen, and volatile fatty acids, which are then utilized by SRB to reduce sulfate [44]. Lactate, which is a co-substrate in this study, is a preferred substrate for both SRB and FAB microbes. Hence, organic carbon is utilized for both sulfate reduction and FAB resulting in TOC removal higher than the quantity of organics required as per the stoichiometric ratio of sulfate reduction. So considering different metabolic pathways, a COD/sulfate mass ratio of about 2.0 is considered optimum

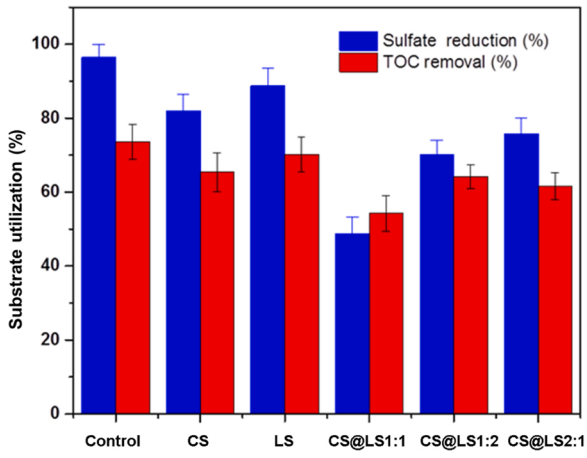

Fig. 3. Sulfidogenic sludge biomass activity exposed to CS, LS and CS@LS (100 μg/mL). Substrate utilization presented as sulfate reduction and TOC removal profiles.

for the bacterial growth and sulfate reduction in batch conditions [45].

The activity of SRBs is assessed by sulfate reduction and co-substrate oxidation since sulfate reduction is considerd an oxidation-reduction reaction, in which sulfate act as an electron acceptor. Accordingly, a suitable and sufficient electron donor is required for the SRBs activities. CS and LS showed a small inhibitory effect on the SRBs activity in terms of sulfate reduction (15.5% and 8.46%, respectively) and TOC utilization (14.3% and 6.3%, respectively). The inhibitory effects of all three NC were higher than the inhibition caused by CS and LS. Further, it was found that the NC CS@LS-1:1showed the highest inhibition of 44.53% and 32.34% for sulfate reduction and co-substrate oxidation, respectively. Thus, different inhibitory effects could be due to the different characteristics of the three NC related to their size, shape, and stability. As reported in the earlier section, CS@LS-1:1 has the smallest hydrodynamic diameter in the aqueous suspension as compared to the other two NC. Moreover, the NC shape is regular, uniform and stable in presence of high salt concentration. So, CS@LS-1:1 showed the highest inhibition of SRBs activity as compared to CS, LS, CS@LS-2:1 and CS@LS-1:2 and was considered as the optimal one for further studies.

3.3. Effect of CS@LS concentrations on SRBs inhibition

As the concentration of 100 μg/mL of CS@LS-1:1 was inhibitory to both anaerobic organics oxidation and sulfate reduction, it was considered important to investigate whether lower and higher concentrations of CS@LS-1:1 have any effect on microbial metabolism. Batch assays were performed to investigate the effects of CS@LS-1:1 concentration between 0 and 500 μg/mL as shown in Fig. 4(A). The residual sulfate concentration in absence of any inhibitor has decreased from 200 mg/L to 4.52 mg/L with a sulfate reduction efficiency of about 98%. Residual sulfate concentration in presence of 20 μg/mL CS@LS-1:1 was pretty stable and similar to those in the absence of CS@LS-1:1 in the control assay. These results indicated that a lower concentration of 20 μg/mL of CS@LS-1:1 had no significant inhibitory effects on SRBs activity. Nevertheless, when SRBs consortia were exposed to a higher concentration of 50–500 μg/mL CS@LS-1:1, the residual sulfate concentrations significantly increased from 4.52 mg/L in control to approximately 174.0 mg/L with increasing CS@LS-1:1 concentration to 500 μg/mL. The sulfate reduction efficiency of assays exposed to 150 μg/mL CS@LS-1:1 was about 36.0% and in presence of 300 μg/mL was about 14%, which was remarkably lower than that in the control (97.4%). Though, further increase in CS@LS-1:1 concentration to 500 μg/mL showed almost the same sulfate reduction profile as that in the presence of 300 μg/mL suggesting that it was the optimal concentration for SRBs inhibition in our experimental setup. Fig. 4(B) shows the specific sulfate reduction rates (SSRR) at different CS@LS-1:1 concentration. As the NC concentration was increased from 50 to 500 μg/mL, the SSRR decreased from 0.278 to 0.036 g-sulfate/g-VSS*day showing a relative sulfate reduction inhibition of 86.64% as compared to that of control.

The sulfate transport takes place because of the concentration gradient of sodium ions and/or protons, and electrical potential across the cell membrane [27]. Dissimilatory sulfate reduction by anaerobic SRBs occurs in three steps. Firstly, intracellular sulfate is activated to adenosine phosphosulfate (APS) by the enzyme ATP sulfurylase. The APS-sulfite redox couple has a favorable redox potential (E0') of − 60 mV, which allows APS to reduce to sulfite with the enzyme APS reductase. Finally, sulfite is reduced to sulfide with the enzyme dissimilatory sulfite reductase (DSR) [28]. The influences of CS@LS-1:1 on the bio-transformations of sulfate to sulfide under the anaerobic sulfidogenic environment were further investigated by analyzing intermediate sulfite and biogenic sulfide production in presence of different inhibitors concentrations. The results obtained at the end of batch assays are presented in Fig. S1. Sulfite was detected as the intermediates of sulfate reduction. The concentration of sulfite was 1.2 mg/L in the control assay, whereas, sulfite concentration gradually increased with

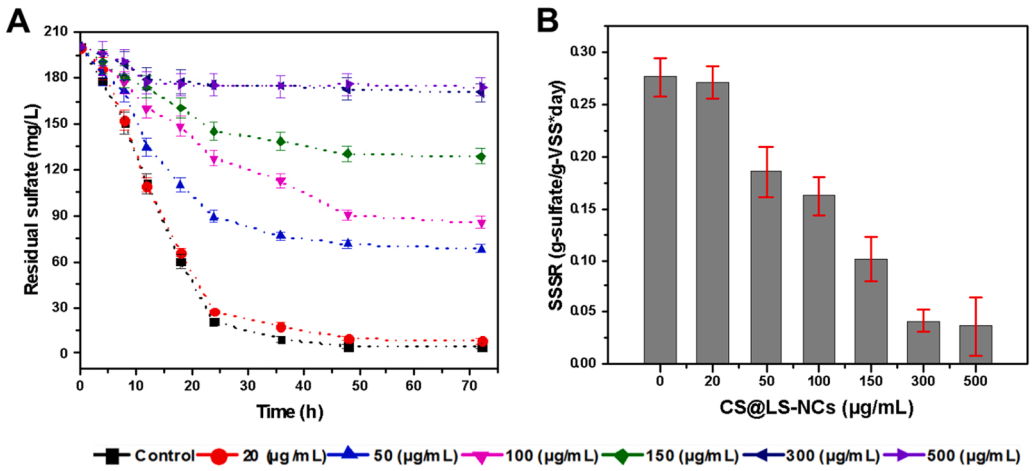

Fig. 4. Activity of anaerobic sulfidogenic mixed consortia (200 mg.VSS/L) exposed to different concentrations of CS@LS-1:1 (0–500 µg/mL) in the inject seawater at 35 °C. (A) Sulfate reduction (B) relative sulfate reduction inhibition as %age of control at different concentrations of CS@LS-1:1 NC. Batch reactor without CS@LS-1:1 NC was used as control.

increasing the inhibitor concentrations and was 10.41 mg/L in presence of the highest CS@LS-1:1 concentration of 500 µg/mL. The accumulation of sulfite in presence of higher CS@LS concentrations might be attributed to sulfidogenic oxidation inhibition. In this study, an increase in sulfite accumulation which is an intermediate product in sulfate reduction indicated that CS@LS-1:1 could significantly inhibit sulfite reduction to sulfide. Moreover, it was observed that sulfide production was significantly different from that of control assays where no nanoparticles were presented (Fig. S2). The concentrations of dissolved sulfide also decreased in the presence of CS@LS and showed a concentration-dependent behavior. Total dissolved sulfide concentration was 28.48 mg/L in absence of any CS@LS and decreased to 8.12 mg/ L in the presence of 500 µg/mL of CS@LS causing a strong inhibition to biogenic sulfide production at higher concentrations of the inhibitor.

Fig. S3 shows the effect of different concentrations of CS@LS-1:1 (0–500 µg/mL) on the sulfur mass balances in terms of sulfur species fractions (residual sulfate-sulfur, sulfite-sulfur and sulfide-sulfur) monitored in this study. Residual sulfate-sulfur started to accumulate at 50 µg/mL of CS@LS-1:1. The residual sulfate-sulfur concentrations significantly increased from 1.50 mg/L in control to 56.85 mg/L in presence of 300 µg/mL of inhibitor and remain almost same at higher concentration of biocide. Meanwhile there was no significant effect of nanocomposite concentration up to 50 µg/mL on sulfite-sulfur component. A concentration of 100 µg/mL of CS@LS-1:1 showed buildup of Sulfite-sulfur, which increased to 8.12 mg/L at 500 µg/mL of biocide. Then, the increase of the residual sulfate resulted in decrease in sulfide-sulfur accumulation in the bioreactor. Sulfur component of dissolved sulfide was 28.48 mg/L in control assay and decreased with increasing concentration of sulfate-sulfur and lowest concentration of 7.4 mg/L was found at 300 µg/mL of NC.

Fig. S4 depicts the effects of CS@LS concentration on the pH of the batch assays. The initial pH of the assays was adjusted to 7.5 before spiking CS@LS-1:1 into the SRBs matrix. The pH of the control assay was 8.16 as expected for the biological sulfate-reduction reaction due to the production of alkalinity. However, the pH decreased to 7.41 in presence of 500 µg/mL CS@LS-1:1. The decrease in the pH values and dissolved sulfide concentrations in presence of NC indicated the inhibition of sulfate-reduction, which eventually resulted in lower alkalinity production. A decrease in sulfide production could be attributed to the accumulation of sulfite during the sulfate reduction process. Nevertheless, it is imperative to indicate that no data on the application of CS/LS-based (NMs) for SRBs inhibition have been found in the literature to compare with our results obtained in this study.

The presence of appropriate and adequate co-substrate (electron donor) is required for the effective reduction of sulfate to sulfide. In this study, lactate was used as co-substrate and the influence of different CS@LS-1:1 concentration on lactate oxidation was assessed by analyzing TOC, Fig. 5(A). The initial average TOC concentration of 150 mg/L was reduced to 18.41 mg/L after 192 h of reaction time in the absence of an inhibitor as the control assay. The average residual TOC concentrations increased from 23.5 to 87.25 mg/L with increasing CS@LS-1:1 concentration from 20 to 500 µg/mL. Therefore, a decrease of co-substrate oxidation was obtained from 87.72% to 41.83% with increasing CS@LS-1:1 concentration from 0 to 500 µg/mL. Moreover, Fig. 5(B) shows the specific organics utilization rate (SOUR) of SRBs in presence of different concentrations of CS@LS-1:1. When the NC concentration was increased from 20 to 500 µg/mL, the SOUR decreased from 0.082 to 0.039 0.036 g-TOC/g-VSS*day giving a relative co-substrate oxidation inhibition of 52.19% as compared to that of control.

It is well-known that anaerobic oxidation of organic compounds with mixed microbial consortia can be achieved by a sequence of biochemical reactions. Lactate could be oxidized to intermediate propionic acid, ethanol, acetic acid, and finally to CO_2. However, accumulation of propionic acid in the biological sulfate reduction process was reported earlier in presence of ZnO-NPs [46], and profiles of co-substrate and its intermediate products showed that ZnO-NPs could significantly affect co-substrate utilization. Inhibition of intermediate propionic acid was attributed to sulfidogenic oxidation inhibition [46]. So, inhibition of co-substrate utilization in this study could be assigned to the accumulation of intermediate organics compound formed after lactate oxidation. The CS@LS are in suspension and are not expected to contribute to the biochemical reaction. Based on the above finding, it was assumed that the CS@LS-1:1 may have inhibited the bacteria through physical interaction and/or due to oxidative stress caused by the production of reactive oxygen species. The CS@LS could act as an obstruction that could stop the interaction of the electron donor-acceptor couple to the active bacterial site and/or can inhibit the enzyme activities causing the sulfate reduction [47].

3.4. Influence of CS@LS on SRBs viability and general physiology

To further evaluate the inhibitory mechanism of CS@LS-1:1 on SRBs biomass, multiple probable number (MPN) tests were carried out after 190 h of reaction time for the assays in the absence and presence of CS@LS-1:1 to determine the count of viable bacterial cells in the batch assays. The MPN experiments showed that the estimated SRBs counts in the control assay (in absence of NC) were 2.1×10^8 per mL. Despite

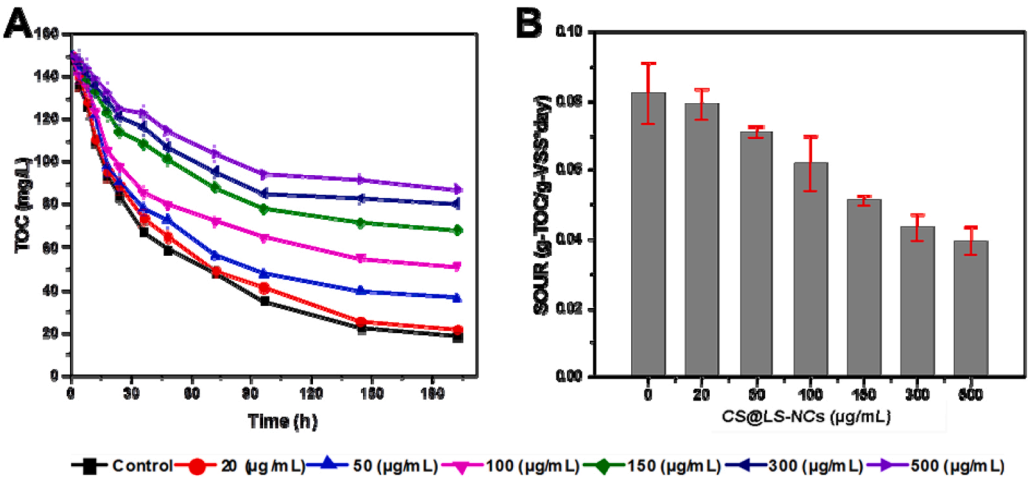

Fig. 5. Activity of anaerobic SRBs mixed consortia (200 mg.VSS/L) treated with different concentrations of CS@LS (0–500 µg/mL) in the inject seawater at 35 °C. (A) Organics oxidation as TOC (B) specific organics utilization rate (SOUR) profiles during 190 h reaction time.

differences in co-substrate oxidation and sulfate reduction rates, the batch assays exposed to 20, 50, 100 and 150 µg/mL CS@LS-1:1 had almost similar bacterial growth counts as compared to that of control. However, the assays spiked with a higher concentration of 300 and 500 µg/mL CS@LS showed a reduction in cell viability, in which, SRBs counts decreased to 1.8×107 and 1.5×10^6 per mL. This can confirm that the SRBs exposed up to 150 µg/mL of NC may not dead but simply deactivated and lost the ability to reduce sulfate. Yet, higher concentrations of NC could result in a significant viability loss of SRBs consortia. The SRBs– CS@LS contact in the well-mixed reactors could be responsible for the deactivation of SRBs bacteria as discussed earlier. The results found in this study were indicated that the metal sulfides and iron nanoparticles showed similar behavior against SRBs at lower concentrations, which is in good agreement with previously reported data [48,49]. Cell viability measurement using cultivation-based methods is not an adequate approach as most of the bacteria could be viable-but-not-culturable and therefore a bimolecular method is advantageous for the better understanding of microorganism's cell viability [50]. The direct estimate of SRBs culture viability was further investigated utilizing flow cytometry measurements (FCM). Because the mixed culture of SRBs used in this study is very diverse and heterogeneous, the use of flow cytometry offers a promising technique for the

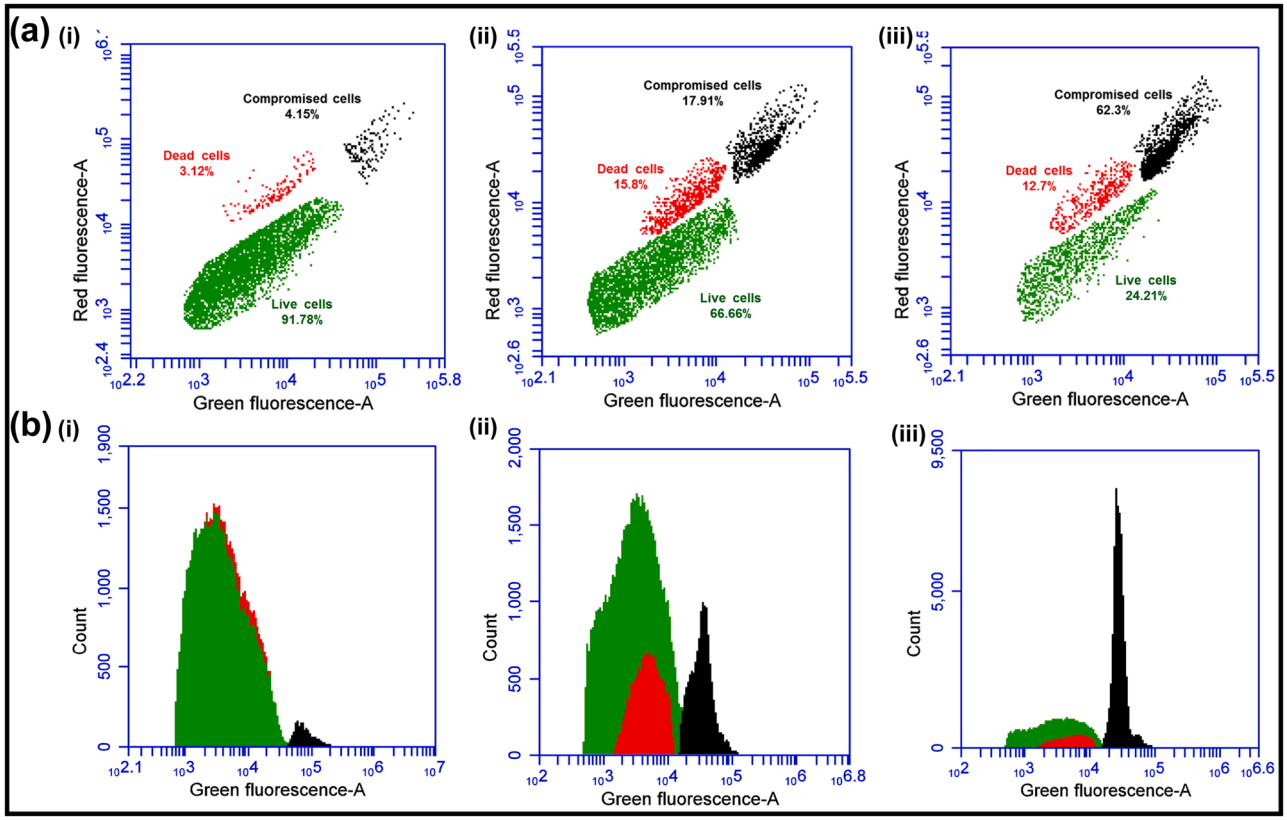

Fig. 6. Red and green fluorescence and forward light scattering distributions of SRBs culture before and after exposure to CS@LS-1:1. (A) Dot plots of green versus red fluorescence of bacterial culture exposed to (i) 0 µg/mL (ii) 300 µg/mL and (iii) 500 µg/mL of CS@LS-1:1. (B) Green fluorescence histograms of viable and dead cells of bacterial culture exposed to (i) 0 µg/mL (ii) 300 µg/mL and (iii) 500 µg/mL of CS@LS-1:1.

analysis of cell viability after exposure to antibacterial materials [51]. In FCM, the term cell viability indicates the cells with intact membranes, which are detected using nucleic acids staining dyes retention or exclusion such as propidium iodide (PI) and SYTO 9. The SYTO 9 is a dye capable of staining all cells, whether living or dead, whereas, the PI is capable of staining only dead or damaged/compromised cells. Fig. 6 shows the cytograms of flow cytometric analysis, in which each cell is represented as a function of green fluorescence and red fluorescence on the horizontal and vertical axis, respectively. Due to the activation of energy transfer phenomenon in presence of SYTO 9 and PI in dead cells, the PI fluorescent emission spectrum absorbs the spectrum of SYTO 9 and thus only PI spectrum is visible. Consequently, viable cells with green fluorescence can be clearly distinguished from dead ones with red fluorescence (Fig. 7(a)). In the compromised cells, both green and red fluorescence is emitted and a third region can be distinguished in the flow cytometry plots (labeled as black color). In the analysis of the experimental data, both cells in red and compromised regions were considered inactive and inhibited cells, which were not able to grow after exposure to synthesized NC. Fig. 6(a & b (i)) shows the dot plots and histogram of control SRBs culture which shows the initial culture was composed of about 92% of viable cells and 3% of dead cells, whereas 4% of the cells were compromised. For the assay exposed to the highest concentration of 500 μg/mL CS@LS-1:1, cell viability decreased to 24%. This decrease in viability did not correspond to an equivalent increase in dead cells, which reached only 12.7%. The decrease in cell viability was balanced by the increase in the compromised and/or damaged cells to 62%. These results indicated that most of the cells were not dead but severely damaged and have lost their ability to reduce sulfate and utilize organic substrate as discussed above.

SEM analysis was performed to study the influence of CS@LS-1:1 on cell biomass surface structure after exposure to CS@LS-1:1. Cells were in good shape, and smooth in absence of CS@LS-1:1 (control assay, Fig. 7 (A)), whereas, in presence of NC large numbers of cells were agglomerated and showed significant surface damage (Fig. 7(B)).

To confirm the SEM observations, an LDH release assay was performed (which is an indicator of cell membrane damage) to determine the SRBs cell's surface integrity. LDH assay exhibited that no measurable cytoplasmic leakage happened after exposure to CS@LS-1:1 concentration up to 100 μg/mL (Fig. 8) confirming that the surface of SRBs was intact. Nonetheless, higher CS@LS-1:1 concentration resulted in significant cytoplasmic leakage and the results are in line with the SRBs viability studies by MPN method. The toxicity of several nanoparticles has been assigned to ROS-dependent or independent oxidative stress induced by NPs [52]. Another possible explanation of the NC toxicity in addition to oxidative stress is cell membrane damage. In this study, the exposure of SRBs consortia to 500 μg/mL CS@LS-1:1 considerably increased the extracellular LDH to 265.5% as compared to that of control, which indicates a substantial cytoplasmic leakage outside the cells.

The formation of biofilm by SRBs may act as a survival strategy in a toxic and nutritionally deficit environment. EPS has an important role in keeping microorganisms together in biofilm complex structure. In this study, we investigated the impact of CS@LS-1:1 –NC on the different constituents of EPS secreted by SRBs consortia, and results are given in Table 1. The protein contents of the SRBs consortia after exposure to 500 μg/mL CS@LS-1:1 was decreased from 3.37 to 1.93 mg/g-VSS, whereas the number of carbohydrates after exposure to CS@LS-1:1 did not show significant differences as compared to that of control. Exposure of the NC also affected the concentrations of humic substances and lipids, which were 2.12 mg/g-VSS and 0.256 mg/g-VSS, respectively, in absence of NC. However, in presence of 500 μg/mL CS@LS-1:1, the contents of both constituents decreased to 1.12 mg/g-VSS and 0.189 mg/g-VSS, respectively. In biofilm formation, proteins are carbon and energy source, whereas, polysaccharides are capable of both adhesion and cohesion interactions. The impact of several nanoparticles on constituents of EPS of diverse bacterial communities has been investigated [53–56]. According to the above investigations, CS@LS caused the significant inhibition to biological sulfate reduction, and organics oxidation and inhibitory effects were dependent on the concentration of the NC. The inhibition of SRBs activity occurred due to the accumulation of sulfite during sulfate reduction and serious inhibition of co-substrate utilization. The SRBs inhibitory effect was due to the decrease in cell viability, serious cytoplasmic leakage, and loss of cell integrity and EPS contents.

Nevertheless, to date, only a few studies have provided actual information on the impact of nanoparticles on SRBs biofilm formation, EPS production, and cell growth inhibition. Additionally, there is limited work available on the use of CS/LS NC as a biocide to inhibit SRBs activity and the impact of NC on EPS contents. Higher inhibitory

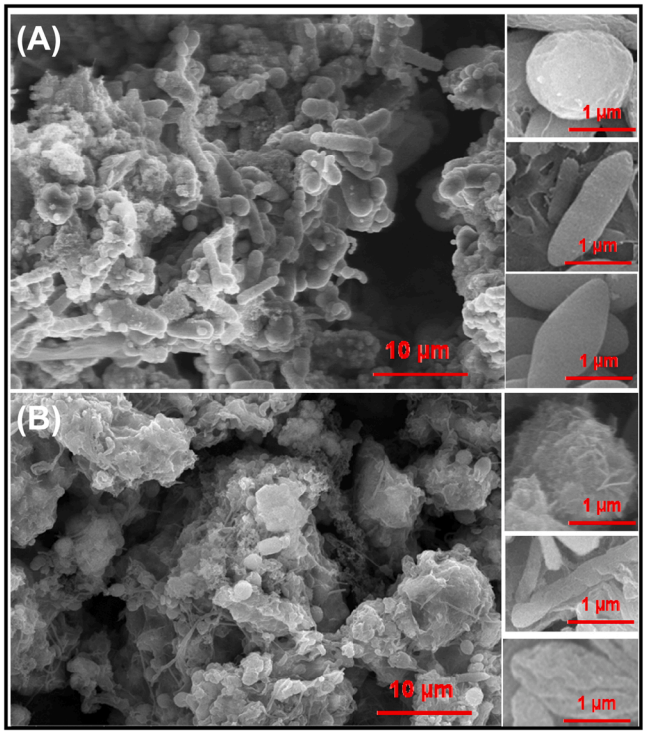

Fig. 7. SEM images of SRBs sludge at lower and higher magnifications (A) control and (B) exposed to 500 μg/mL CS@LS-1:1.

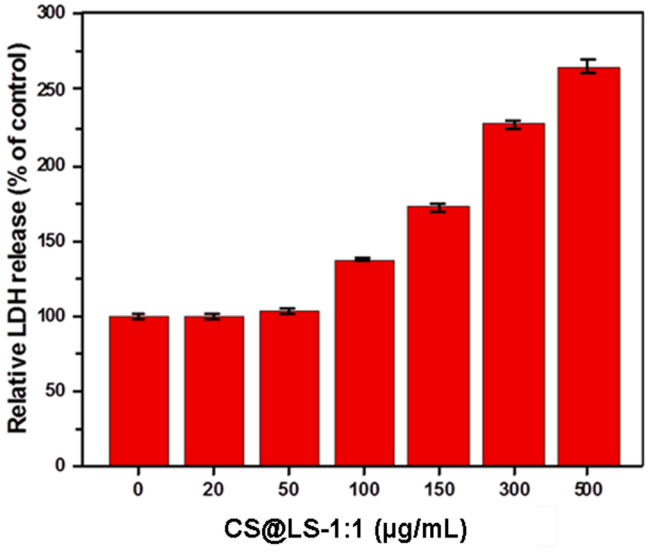

Fig. 8. Lactate dehydrogenase release from sulfidogenic biofilm treated with different concentrations of CS@LS-1:1 NC.

Table 1
Analysis of EPS extracted from sulfidogenic biomass exposed to different concentrations of CS@LS (0–500 μg/mL) at 35 °C.

CS@LS (μg/mL)	Carbohydrates (mg/g)	Proteins (mg/g)	Humic substances (mg/g)	Lipids (mg/g)
0	53.8	3.37	2.12	0.256
20	53.21	3.36	2.12	0.251
50	50.26	3.25	1.95	0.234
100	47.37	2.62	1.54	0.218
150	45.94	2.21	1.378	0.207
300	44.38	1.94	1.12	0.197
500	43.32	1.93	1.07	0.189

effects of CS@LS can be attributed to the synergy between nano-size effect and the presence of large number of amino groups which make the NC hydrophilic and bio-adhesive binding readily to negatively charged bacterial cell surfaces leading to membrane disruption and cell death [57].

3.5. Acute toxicity and impact of CS@LS on zebrafish embryos

NMs, depending on their particle size and morphology, have the potential to easily enter the bodies of living organisms including human beings, and can reach the most sensitive organs such as lungs, liver, heart, spleen, and brain. This interaction may result in interference of the cell's normal biochemical environments [58]. Therefore, testing of CS@LS-1:1 for the potentially harmful effects on living organisms is important before using the NC for waster disinfection applications. We investigated the acute toxicology of the cross-linked CS@LS-1:1 and the CS/LS blend according to the acute toxicity assay adapted from the Organization for Economic Co-operation and Development (OECD) guideline for testing chemical toxicity (Nº 203 and 236). The tested concentrations (0, 25, 50, 100, 150, 200, 250 μg/mL) that we selected in this study have significant environmental relevance. These concentrations were chosen to be parallel and within the testing scale of the Fish and Wildlife Service Acute Toxicity Rating Scale [29,32]. It classifies compound's toxicity according to LC_{50} as follow: highly toxic from 0.1 − 1.0 μg/mL, 1.0–10 μg/mL moderately toxic, 10–100 μg/mL slightly toxic, 100–1000 μg/mL practically nontoxic, and > 1000 μg/mL is relatively harmless. In our study, the LC_{50}, was calculated by fitting sigmoidal curve to mortality results using the following equation, y = Bot + (Top-Bot) / [1 + 10 ^ {k * (X0 –Log(C))]. Bot, minimum mortality; Top, maximum mortality; k, curve slope; X0 and LC_{50} were estimated from the mortality curve (Fig. 9D). The LC_{50} for the positive control DEAB was 2.5 μM, and for the CS@LS was 103.3 μg/mL. However, for non-cross-linked CS/LS, the LC_{50} was much higher than the CS@LS (584.8 μg/mL). Thus, according to the Fish and Wildlife Service Acute Toxicity Rating Scale [29,32], both nanoparticles can be classified as "practically not toxic". At 72-hpf, the NOEC (the concentration where >80% of the embryos survived and did not show deformities) for the CS@LS-1:1 was between 50 and 100 μg/mL (Fig. 9 C). At 50 μg/mL CS@LS-1:1, no significant sign of body deformities was recorded (similar to the negative control, Fig. 9B)]. However,100 μg/mL concentration of CS@LS, 24% were dead and 19% of the embryos started to show deformities, such as yolk and heart edema found in the DEAB positive control (Fig. 9B). On the other hand, for blended CS and LS suspension, the NOEC was higher than CS@LS-1:1 NC, between 150 − 200 μg/mL. It is noteworthy that at high concentrations of both CS@LS (>150 μg/mL) and CS, LS (>250 μg/mL), around 10% of the embryos become hyperactive, a teratogenic phenotype associated with CS nanoparticles that we had observed in the previous study [33]. The lower NOEC and LC_{50} demonstrated by the CS, LS over the CS@LS-1:1 could be due to many reasons. For example, the dechorionated embryo can uptake up to nanoparticles with size 50 nm or less by the skin and up to 700 nm by only oral digestion[59]. Thus at 72-hpf, the only way that nanoparticles to enter the body of the dechorionated embryos is by their permeable skin, because their oral cavities did not open until 96-hpf [59]. The CS@LS-1:1 may have formed a compact that is smaller and able to disperse in aqueous media better than the blended CS/LS suspensions. Therefore, CS@LS were able to penetrate the skin of the embryos and causing more toxicity than CS/LS. We have shown previously that CS and other CS derivatives such as ZnO/CS are eco-friendly

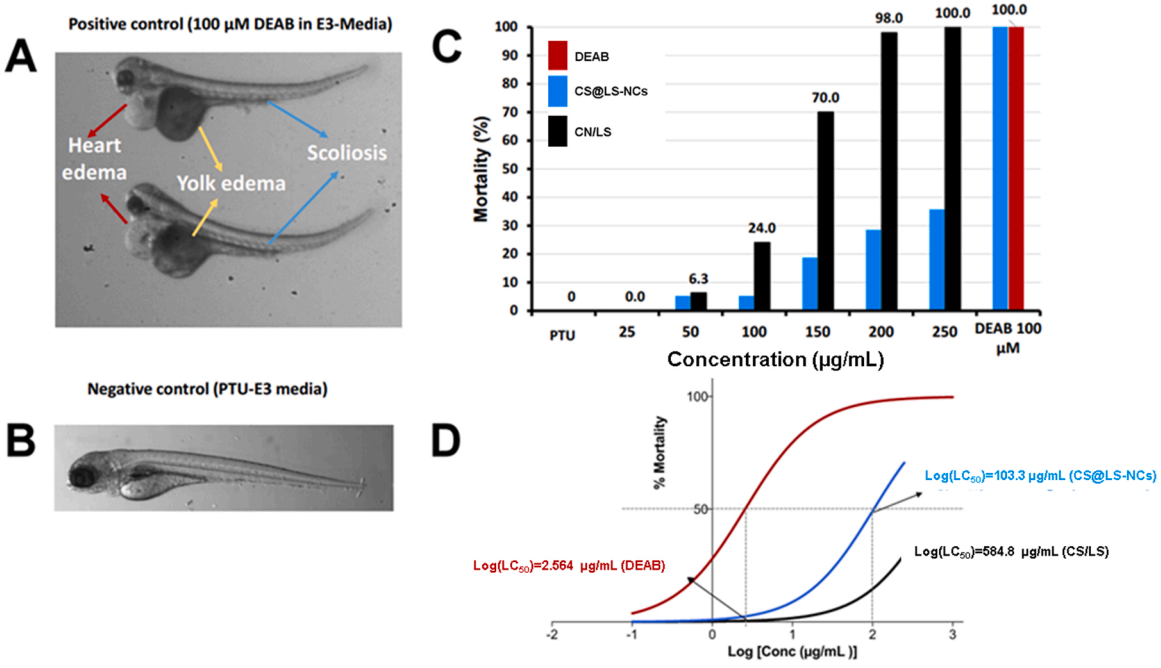

Fig. 9. Representative pictures (72-hpf) of acute toxicity experiments of embryos exposed to (A) 100 μDEAB as positive control, and (B) negative control PTU-E3 media alone. Note the normal embryo in the negative control versus the deformed embryos in the positive control (small size, yolk, cardiac edema, and scoliosis. (C) Acute toxicity and survival rate of embryos exposed at different concentrations of DEAB, CS@LS, and blended CS/LS. (D) Mortality response curve where 50 embryos were used in each concentration ($n = 50$).

nanoparticles [33,35]. However, at high concentrations, these nanoparticles have potential organ-specific toxicity. Similarly, it would be pivotal to study the potential organ and cellular toxicity mechanisms of CS@LS-1:1 excreted after long time exposure and at higher concentrations. To sum up, practically studied lower concentrations of CS@LS can be practically classified as not toxic with long-term stability and excellent antibacterial properties against SRBs biofilm. Accordingly, CS@LS NC is potentially useful for controlling the problems of biofilm growth in harsh marine, aquatic environments and inhibition of MIC.

4. Conclusion

We have investigated the inhibitory mode of action of the eco-friendly and biodegradable chitosan/lignosulfonate (CS@LS) based nanocomposite (NC) for the growth inhibition of the SRBs in seawater media. The NC with an average size of 150–200 nm exhibited excellent antibacterial characteristics against SRBs growth and is thus potentially useful for controlling the biofilm growth in highly saline marine and aquatic environments. CS@LS NC depicted concentration-dependent biofilm inhibition and 500 μg/mL of NC showed a relative sulfate reduction inhibition of 86.64% and co-substrate oxidation inhibition of 52.19% as compared to that of control. SRBs growth inhibition and inactivation was further confirmed by multiple probable number counts, SEM, and extracted LDH analysis. Acute toxicity assays using zebrafish embryo model revealed that CS@LS could be classified as environment friendly as per the Fish and Wildlife Service Acute Toxicity Rating Scale. The demonstrated biofilm growth inhibition of CS@LS against SRBs and the practical nontoxicity promotes their potential application as a green biocide in water/wastewater treatment processes and other environmental remediation applications.

CRediT authorship Contribution Statement

Kashif Rasool: Conceptualization, Methodology, Investigation, Validation, Writing- Original draft preparation. **Ravi P. Pandey:** Methodology, Investigation, Validation, Writing- Original draft preparation. **P Abdul Rasheed:** Investigation, Validation, Writing- Reviewing and Editing. **Tricia Gomez:** Investigation, Writing- Reviewing and Editing. **Enas S. Al-Absi:** Investigation, Writing- Reviewing and Editing. Gheyath K. Nasrallah: Conceptualization, Validation, Writing- Reviewing and Editing. **Khaled A Mahmoud:** Conceptualization, Funding acquisition, Supervision, Writing- Reviewing and Editing.

Author Contributions

The manuscript was written through contributions of all authors. All authors have given approval to the final version of the manuscript.

Synopsis

A green and biodegradable chitosan/lignosulfonate nanocomposite is efficient for the inhibition of sulfate-reducing bacteria in seawater media with no toxicity on the marine biota.

Declaration of Competing Interest

The authors declare that they have no known competing financial interests or personal relationships that could have appeared to influence the work reported in this paper.

Acknowledgments

The authors are grateful for the financial support from NPRP grant (NPRP8-286-02-118) from the Qatar National Research Fund (a member of Qatar Foundation). The findings achieved herein are solely the responsibility of the authors. The authors are thankful to J. Ponraj, M Helal, and M. Pasha at the Core lab of QEERI/HBKU, Doha, Qatar for TEM and SEM analysis, respectively. Open Access funding provided by the Qatar National Library.

Appendix A. Supporting information

Supplementary data associated with this article can be found in the online version at doi:10.1016/j.jece.2021.106624.

References

[1] X. Sheng, Y.-P. Ting, S.O. Pehkonen, Evaluation of an organic corrosion inhibitor on abiotic corrosion and microbiologically influenced corrosion of mild steel, Ind. Eng. Chem. Res. 46 (22) (2007) 7117–7125, https://doi.org/10.1021/ie070669f.
[2] X. Sheng, Y.P. Ting, S.O. Pehkonen, Force measurements of bacterial adhesion on metals using a cell probe atomic force microscope, J. Colloid Interface Sci. 310 (2) (2007) 661–669, https://doi.org/10.1016/j.jcis.2007.01.084.
[3] P.A. Rasheed, K.A. Jabbar, H.R. Mackey, K.A. Mahmoud, Recent advancements of nanomaterials as coatings and biocides for the inhibition of sulfate reducing bacteria induced corrosion, Curr. Opin. Chem. Eng. 25 (2019) 35–42, https://doi.org/10.1016/j.coche.2019.06.003.
[4] D. Wan, S. Yuan, K.G. Neoh, E.T. Kang, Surface functionalization of copper via oxidative graft polymerization of 2,2′-bithiophene and immobilization of silver nanoparticles for combating biocorrosion, ACS Appl. Mater. Interfaces 2 (6) (2010) 1653–1662, https://doi.org/10.1021/am100186n.
[5] R. Liang, D.F. Aktas, E. Aydin, V. Bonifay, J. Sunner, J.M. Suflita, Anaerobic biodegradation of alternative fuels and associated biocorrosion of carbon steel in marine environments, Environ. Sci. Technol. 50 (9) (2016) 4844–4853, https://doi.org/10.1021/acs.est.5b06388.
[6] C.N. Lyles, D.F. Aktas, K.E. Duncan, A.V. Callaghan, B.S. Stevenson, J.M. Suflita, Impact of organosulfur content on diesel fuel stability and implications for carbon steel corrosion, Environ. Sci. Technol. 47 (11) (2013) 6052–6062, https://doi.org/10.1021/es4006702.
[7] C. Lyles, H. Le, W. Beasley, M. McInerney, J. Suflita, Anaerobic hydrocarbon and fatty acid metabolism by syntrophic bacteria and their impact on carbon steel corrosion, Front. Microbiol. 5 (114) (2014), https://doi.org/10.3389/fmicb.2014.00114.
[8] L. Boulané-Petermann, Processes of bioadhesion on stainless steel surfaces and cleanability: a review with special reference to the food industry, Biofouling 10 (4) (1996) 275–300, https://doi.org/10.1080/08927019609386287.
[9] A. Boyd, A.M. Chakrabarty, Pseudomonas aeruginosa biofilms: role of the alginate exopolysaccharide, J. Ind. Microbiol. 15 (3) (1995) 162–168, https://doi.org/10.1007/bf01569821.
[10] J.F. Batista, R.F.C. Pereira, J.M. Lopes, M.F.M. Carvalho, M.J. Feio, M.A.M. Reis, In situ corrosion control in industrial water systems, Biodegradation 11 (6) (2000) 441–448, https://doi.org/10.1023/a:1011620023116.
[11] T. Wang, D. Zhang, L. Dai, Y. Chen, X. Dai, Effects of metal nanoparticles on methane production from waste-activated sludge and microorganism community shift in anaerobic granular sludge, Sci. Rep. 6 (2016) 25857. ⟨https://doi.org/10.1038/srep25857⟩. https://www.nature.com/articles/srep25857#supplementary-information.
[12] F. Pan, W. Liu, Y. Yu, X. Yin, Q. Wang, Z. Zheng, M. Wu, D. Zhao, Q. Zhang, X. Lei, D. Xia, The effects of manganese oxide octahedral molecular sieve chitosan microspheres on sludge bacterial community structures during sewage biological treatment, Sci. Rep. 6 (2016) 37518. ⟨https://doi.org/10.1038/srep37518⟩. https://www.nature.com/articles/srep37518#supplementary-information.
[13] K. Meli, I. Kamika, J. Keshri, M.N.B. Momba, The impact of zinc oxide nanoparticles on the bacterial microbiome of activated sludge systems, Sci. Rep. 6 (2016) 39176, https://doi.org/10.1038/srep39176.
[14] M. Simonin, A. Richaume, J.P. Guyonnet, A. Dubost, J.M.F. Martins, T. Pommier, Titanium dioxide nanoparticles strongly impact soil microbial function by affecting archaeal nitrifiers, Sci. Rep. 6 (2016) 33643. ⟨https://doi.org/10.1038/srep33643⟩. https://www.nature.com/articles/srep33643#supplementary-information.
[15] T. Xia, M. Kovochich, M. Liong, L. Mädler, B. Gilbert, H. Shi, J.I. Yeh, J.I. Zink, A. E. Nel, Comparison of the mechanism of toxicity of zinc oxide and cerium oxide nanoparticles based on dissolution and oxidative stress properties, ACS Nano 2 (10) (2008) 2121–2134, https://doi.org/10.1021/nn800511k.
[16] K. Rasool, M. Helal, A. Ali, C.E. Ren, Y. Gogotsi, K.A. Mahmoud, Antibacterial activity of Ti3C2Tx MXene, ACS Nano 10 (3) (2016) 3674–3684, https://doi.org/10.1021/acsnano.6b00181.
[17] M.A. Maurer-Jones, I.L. Gunsolus, C.J. Murphy, C.L. Haynes, Toxicity of engineered nanoparticles in the environment, Anal. Chem. 85 (6) (2013) 3036–3049, https://doi.org/10.1021/ac303636s.
[18] G. López-Carballo, L. Higueras, R. Gavara, P. Hernández-Muñoz, Silver ions release from antibacterial chitosan films containing in situ generated silver nanoparticles, J. Agric. Food Chem. 61 (1) (2013) 260–267, https://doi.org/10.1021/jf304006y.
[19] A. Regiel-Futyra, M. Kus-Liśkiewicz, V. Sebastian, S. Irusta, M. Arruebo, G. Stochel, A. Kyzioł, Development of noncytotoxic chitosan–gold nanocomposites as efficient antibacterial materials, ACS Appl. Mater. Interfaces 7 (2) (2015) 1087–1099, https://doi.org/10.1021/am508094e.

[20] E.I. Rabea, M.E.T. Badawy, C.V. Stevens, G. Smagghe, W. Steurbaut, Chitosan as antimicrobial agent: applications and mode of action, Biomacromolecules 4 (6) (2003) 1457–1465, https://doi.org/10.1021/bm034130m.
[21] H. Wang, J. Qian, F. Ding, Emerging chitosan-based films for food packaging applications, J. Agric. Food Chem. (2017), https://doi.org/10.1021/acs.jafc.7b04528.
[22] J.H. Lora, W.G. Glasser, Recent industrial applications of lignin: a sustainable alternative to nonrenewable materials, J. Polym. Environ. 10 (1) (2002) 39–48, https://doi.org/10.1023/a:1021070006895.
[23] R.P. Pandey, K. Rasool, P.A. Rasheed, T. Gomez, M. Pasha, S.A. Mansour, O.-S. Lee, K.A. Mahmoud, One-step synthesis of an antimicrobial framework based on covalently cross-linked chitosan/lignosulfonate (CS@LS) nanospheres, Green. Chem. (2020), https://doi.org/10.1039/C9GC03461G.
[24] P.A. Rasheed, R.P. Pandey, K.A. Jabbar, A. Samara, A.M. Abdullah, K.A. Mahmoud, Chitosan/lignosulfonate nanospheres as "Green" biocide for controlling the microbiologically influenced corrosion of carbon steel, Materials (Basel) 13 (11) (2020) 2484, https://doi.org/10.3390/ma13112484.
[25] M. Chandrasekaran, K.D. Kim, S.C. Chun, Antibacterial activity of chitosan nanoparticles: a review, Processes 8 (9) (2020) 1173.
[26] M.S. Riaz Rajoka, H.M. Mehwish, Y. Wu, L. Zhao, Y. Arfat, K. Majeed, S. Anwaar, Chitin/chitosan derivatives and their interactions with microorganisms: a comprehensive review and future perspectives, Crit. Rev. Biotechnol. 40 (3) (2020) 365–379, https://doi.org/10.1080/07388551.2020.1713719.
[27] Z.Z. Zakaria, F.M. Benslimane, G.K. Nasrallah, S. Shurbaji, N.N. Younes, F. Mraiche, S.I. Da'as, H.C. Yalcin, Using zebrafish for Investigating the molecular mechanisms of drug-induced cardiotoxicity, BioMed. Res. Int. (2018).
[28] R.P. Pandey, K. Rasool, P.A. Rasheed, T. Gomez, M. Pasha, S.A. Mansour, O.-S. Lee, K.A. Mahmoud, One-step synthesis of an antimicrobial framework based on covalently cross-linked chitosan/lignosulfonate (CS@LS) nanospheres, Green. Chem. 22 (3) (2020) 678–687, https://doi.org/10.1039/C9GC03461G.
[29] P.A. Rasheed, R.P. Pandey, K. Rasool, K.A. Mahmoud, Ultra-sensitive electrocatalytic detection of bromate in drinking water based on Nafion/Ti3C2Tx (MXene) modified glassy carbon electrode, Sens. Actuators B: Chem. 265 (2018) 652–659, https://doi.org/10.1016/j.snb.2018.03.103.
[30] K. Rasool, D.S. Lee, Characteristics, kinetics and thermodynamics of Congo Red biosorption by activated sulfidogenic sludge from an aqueous solution, Int. J. Environ. Sci. Technol. (2013), https://doi.org/10.1007/s13762-013-0462-2.
[31] K. Rasool, D.S. Lee, Inhibitory effects of silver nanoparticles on removal of organic pollutants and sulfate in an anaerobic biological wastewater treatment process, J. Nanosci. Nanotechnol. 16 (5) (2016) 4456–4463, https://doi.org/10.1166/jnn.2016.10984.
[32] N. Younes, R. Salem, M. Al-Asmakh, T. Altamash, G. Pintus, M. Khraisheh, G. K. Nasrallah, Toxicity evaluation of selected ionic liquid compounds on embryonic development of Zebrafish, Electronic (2018) 1090–2414.
[33] H. Abou-Saleh, N. Younes, K. Rasool, M.H. Younis, R.M. Prieto, H.M. Yassine, K. A. Mahmoud, G. Pintus, G.K. Nasrallah, Impaired liver size and compromised neurobehavioral activity are elicited by chitosan nanoparticles in the zebrafish embryo model, Nanomaterials 9 (1) (2019) 122.
[34] G. Nasrallah, R. Salem, S. Da'as, O.L.A. Al-Jamal, M. Scott, I. Mustafa, Biocompatibility and toxicity of novel iron chelator Starch-Deferoxamine (S-DFO) compared to zinc oxide nanoparticles to zebrafish embryo: an oxidative stress based apoptosis, physicochemical and neurological study profile, Neurotoxicology Teratol. (2019).
[35] N. Younes, G. Pintus, M. Al-Asmakh, K. Rasool, S. Younes, S. Calzolari, K. A. Mahmoud, G. Nasrallah, "Safe" chitosan zinc oxide nanocomposite has minimal organ-specific toxicity on early stages of zebrafish development, ACS Biomater. Sci. Eng. (2019).
[36] X. Ouyang, W. Wang, Q. Yuan, S. Li, Q. Zhang, P. Zhao, Improvement of lignin yield and purity from corncob in the presence of steam explosion and liquid hot pressured alcohol, RSC Adv. 5 (76) (2015) 61650–61656, https://doi.org/10.1039/C5RA12452B.
[37] Y. Wang, A. Pitto-Barry, A. Habtemariam, I. Romero-Canelon, P.J. Sadler, N.P. E. Barry, Nanoparticles of chitosan conjugated to organo-ruthenium complexes, Inorg. Chem. Front. 3 (8) (2016) 1058–1064, https://doi.org/10.1039/C6QI00115G.
[38] R.P. Pandey, V.K. Shahi, Aliphatic-aromatic sulphonated polyimide and acid functionalized polysilsesquioxane composite membranes for fuel cell applications, J. Mater. Chem. A 1 (45) (2013) 14375–14383, https://doi.org/10.1039/C3TA12755A.
[39] R.P. Pandey, A.K. Thakur, V.K. Shahi, Stable and efficient composite anion-exchange membranes based on silica modified poly(ethyleneimine)–poly(vinyl alcohol) for electrodialysis, J. Membr. Sci. 469 (2014) 478–487, https://doi.org/10.1016/j.memsci.2014.06.046.
[40] A. Reznickova, N. Slavikova, Z. Kolska, K. Kolarova, T. Belinova, M. Hubalek Kalbacova, M. Cieslar, V. Svorcik, PEGylated gold nanoparticles: stability, cytotoxicity and antibacterial activity, Colloids Surf. A: Physicochem. Eng. Asp. 560 (2019) 26–34, https://doi.org/10.1016/j.colsurfa.2018.09.083.
[41] I. Fernando, T. Qian, Y. Zhou, Long term impact of surfactants & polymers on the colloidal stability, aggregation and dissolution of silver nanoparticles, Environ. Res. 179 (2019), 108781, https://doi.org/10.1016/j.envres.2019.108781.
[42] S. Skoglund, E. Blomberg, I.O. Wallinder, I. Grillo, J.S. Pedersen, L.M. Bergström, A novel explanation for the enhanced colloidal stability of silver nanoparticles in the presence of an oppositely charged surfactant, Phys. Chem. Chem. Phys. 19 (41) (2017) 28037–28043, https://doi.org/10.1039/C7CP04662F.
[43] P.N.L. Lens, A. Visser, A.J.H. Janssen, L.W.H. Pol, G. Lettinga, Biotechnological treatment of sulfate-rich wastewaters, Crit. Rev. Environ. Sci. Technol. 28 (1) (1998) 41–88, https://doi.org/10.1080/10643389891254160.
[44] S. Kalyuzhnyi, V. Fedorovich, P. Lens, L. Hulshoff Pol, G. Lettinga, Mathematical modelling as a tool to study population dynamics between sulfate reducing and methanogenic bacteria, Biodegradation 9 (3) (1998) 187–199, https://doi.org/10.1023/A:1008339018423.
[45] Y. Zhao, N. Ren, A. Wang, Contributions of fermentative acidogenic bacteria and sulfate-reducing bacteria to lactate degradation and sulfate reduction, Chemosphere 72 (2) (2008) 233–242, https://doi.org/10.1016/j.chemosphere.2008.01.046.
[46] K. Rasool, D.S. Lee, Effect of ZnO nanoparticles on biodegradation and biotransformation of co-substrate and sulphonated azo dye in anaerobic biological sulfate reduction processes, Int. Biodeterior. Biodegrad. 109 (2016) 150–156, https://doi.org/10.1016/j.ibiod.2016.01.015.
[47] K.L. Keller, B.J. Rapp-Giles, E.S. Semkiw, I. Porat, S.D. Brown, J.D. Wall, New model for electron flow for sulfate reduction in Desulfovibrio alaskensis G20, Appl. Environ. Microbiol. 80 (3) (2014) 855–868, https://doi.org/10.1128/aem.02963-13.
[48] V.P. Utgikar, S.M. Harmon, N. Chaudhary, H.H. Tabak, R. Govind, J.R. Haines, Inhibition of sulfate-reducing bacteria by metal sulfide formation in bioremediation of acid mine drainage, Environ. Toxicol. 17 (1) (2002) 40–48, https://doi.org/10.1002/tox.10031.
[49] R.J. Barnes, O. Riba, M.N. Gardner, A.C. Singer, S.A. Jackman, I.P. Thompson, Inhibition of biological TCE and sulphate reduction in the presence of iron nanoparticles, Chemosphere 80 (5) (2010) 554–562, https://doi.org/10.1016/j.chemosphere.2010.04.033.
[50] G. Nebe-von-Caron, P.J. Stephens, C.J. Hewitt, J.R. Powell, R.A. Badley, Analysis of bacterial function by multi-colour fluorescence flow cytometry and single cell sorting, J. Microbiol. Methods 42 (1) (2000) 97–114, https://doi.org/10.1016/S0167-7012(00)00181-0.
[51] G. Ziglio, G. Andreottola, S. Barbesti, G. Boschetti, L. Bruni, P. Foladori, R. Villa, Assessment of activated sludge viability with flow cytometry, Water Res. 36 (2) (2002) 460–468, https://doi.org/10.1016/S0043-1354(01)00228-7.
[52] F. Joris, B.B. Manshian, K. Peynshaert, S.C. De Smedt, K. Braeckmans, S.J. Soenen, Assessing nanoparticle toxicity in cell-based assays: influence of cell culture parameters and optimized models for bridging the in vitro–in vivo gap, Chem. Soc. Rev. 42 (21) (2013) 8339–8359, https://doi.org/10.1039/C3CS60145E.
[53] S.-Q. Ni, J. Ni, N. Yang, J. Wang, Effect of magnetic nanoparticles on the performance of activated sludge treatment system, Bioresour. Technol. 143 (2013) 555–561, https://doi.org/10.1016/j.biortech.2013.06.041.
[54] J. Hou, L. Miao, C. Wang, P. Wang, Y. Ao, B. Lv, Effect of CuO nanoparticles on the production and composition of extracellular polymeric substances and physicochemical stability of activated sludge flocs, Bioresour. Technol. 176 (2015) 65–70, https://doi.org/10.1016/j.biortech.2014.11.020.
[55] T. Yadav, A.A. Mungray, A.K. Mungray, Effect of TiO2 nanoparticles on UASB biomass activity and dewatered sludge, Environ. Technol. 38 (4) (2017) 413–423, https://doi.org/10.1080/09593330.2016.1196738.
[56] C. Zhang, Z. Liang, Z. Hu, Bacterial response to a continuous long-term exposure of silver nanoparticles at sub-ppm silver concentrations in a membrane bioreactor activated sludge system, Water Res. 50 (2014) 350–358, https://doi.org/10.1016/j.watres.2013.10.047.
[57] S.R. Saptarshi, A. Duschl, A.L. Lopata, Interaction of nanoparticles with proteins: relation to bio-reactivity of the nanoparticle, J. Nanobiotechnology 11 (1) (2013) 26, https://doi.org/10.1186/1477-3155-11-26.
[58] H. Bahadar, F. Maqbool, K. Niaz, M. Abdollahi, Toxicity of nanoparticles and an overview of current experimental models, Iran. Biomed. J. 20 (1) (2016) 1–11, https://doi.org/10.7508/ibj.2016.01.001.
[59] M. Van Pomeren, N. Brun, W. Peijnenburg, M. Vijver, Exploring uptake and biodistribution of polystyrene (nano) particles in zebrafish embryos at different developmental stages, Aquat. Toxicol. 190 (2017) 40–45.